Spin excitations in metallic kagome lattice FeSn and CoSn

Yaofeng Xie, Lebing Chen, Tong Chen, Qi Wang, Qiangwei Yin, J. Ross Stewart, Matthew B. Stone, Luke L. Daemen, Erxi Feng, Huibo Cao, Hechang Lei, Zhiping Yin, Allan H. MacDonald, and Pengcheng Dai

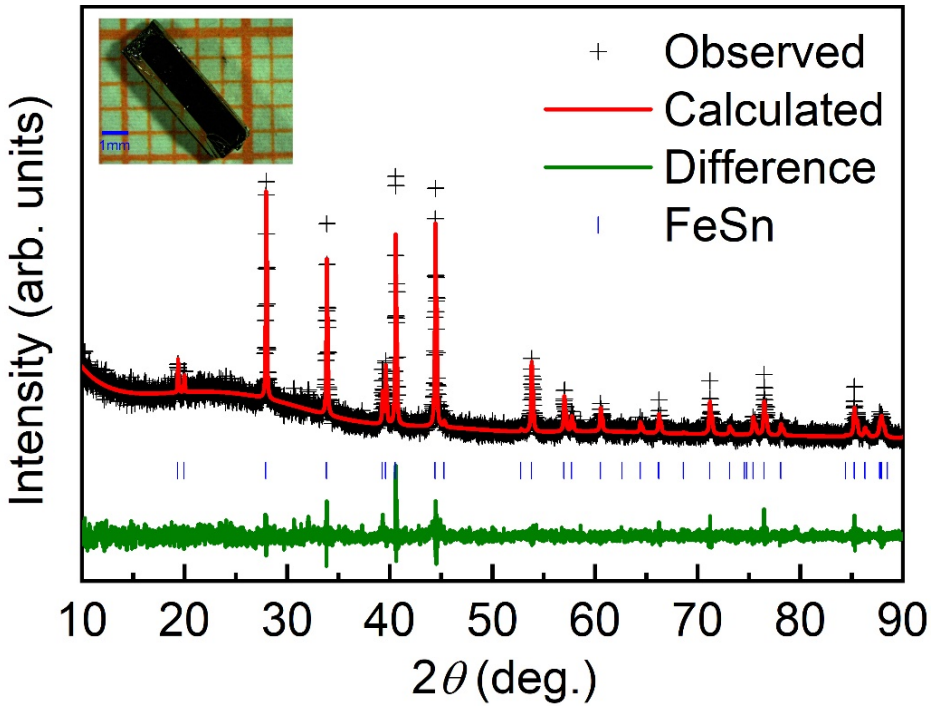

Figure S1. XRD pattern of ground FeSn single crystals. It can be fitted well by using the structure of FeSn with the space group *P*6/*mmm* (No. 191). Inset: photo of typical FeSn single crystal on 1 mm-grid paper.

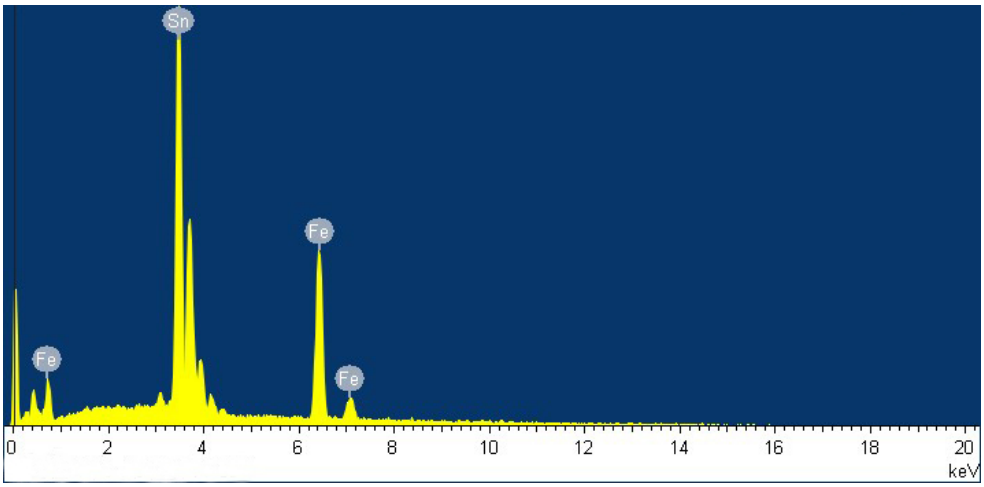

Figure S2. EDX pattern of a FeSn single crystal. Only Fe and Sn elements can be identified.

Table S1. The atomic ratio of Fe:Sn determined from the EDX measurement when setting Sn as 1 for five crystals after polishing the sample surface using sand papers. The average stoichiometry of each crystal is determined by examining 5 different locations on the sample surface. The average compositions of five crystals are very close to the chemical formula of FeSn, indicating negligible Fe vacancies or excess Sn in FeSn crystals.

Sample No. #	Position 1	Position 2	Position 3	Position 4	Position 5	Average
1	0.999:1	0.970:1	1.012:1	0.972:1	0.994:1	0.99(2):1
2	0.962:1	1.000:1	1.043:1	1.004:1	1.035:1	1.01(3):1
3	1.019:1	0.975:1	0.974:1	0.962:1	0.987:1	0.98(2):1
4	0.984:1	0.992:1	0.974:1	1.069:1	1.035:1	1.01(4):1
5	1.044:1	0.995:1	0.955:1	0.971:1	1.027:1	1.00(4):1

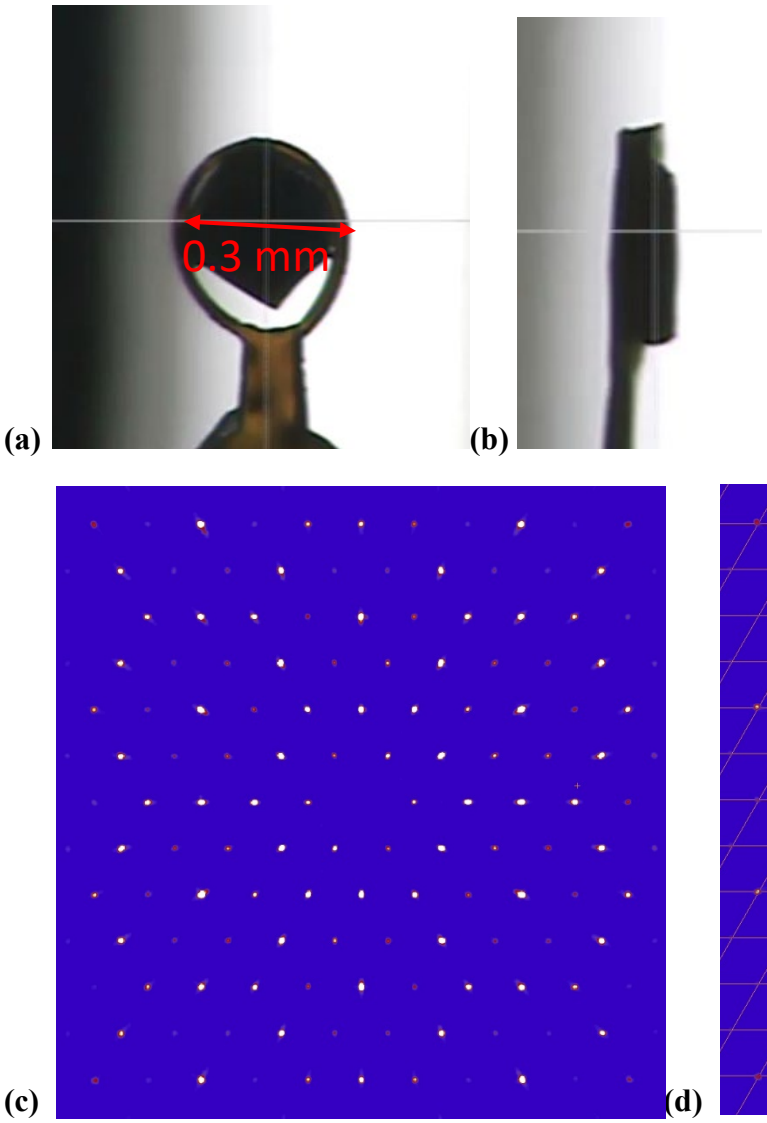

Figure S3. (**a,b**) Pictures of one FeSn single crystal studied by X-ray single crystal refinement. (**c,d**) X-ray diffraction pattern in the [*H*,*K*,0] scattering plane without and with grid.

Table S2. Summary of X-ray single crystal refinement results carried out at 250 K with space group: P_6/mmm (IT: #191). Occupancies of Fe and Sn at 3f site are refined, while Sn at 1a and 2d sites are fixed at 100%. U values are anisotropic Debye-Waller factors.

	Crystal 1	Crystal 2
a (Å)	5.2896(2)	
c (Å)	4.4477 (2)	
T (K)	250	
No. (total reflections)	2887	2919
No. (Unique reflections)	145	144
R_{int}(%)	5.03	9.26
R_{F^2} (%)	2.26	5.79
R_{F^2w} (%)	3.19	7.39
R_F (%)	1.29	2.86
χ^2	0.514	0.68
Sn on Fe (site 3f)	1.2(4) %	1.2(5) %
Fe (Å^2):	U_{11} = 0.0082(5), U_{22}=0.0082(4), U_{33}=0.0080(3), U_{12}=0.0041(4), U_{13} = U_{23}=0, U_{equiv}=0.0081(4)	
Sn1 (Å^2):	U_{11} = 0.0074(4), U_{22}=0.0074(4), U_{33}=0.0135(3), U_{12}=0.0037(4), U_{13} = U_{23}=0, U_{equiv}=0.0095(4)	
Sn2 (Å^2):	U_{11} = 0.0091(4), U_{22}=0.0091(4), U_{33}=0.0067(3), U_{12}=0.0046(4), U_{13} = U_{23}=0, U_{equiv}=0.0083(4)	

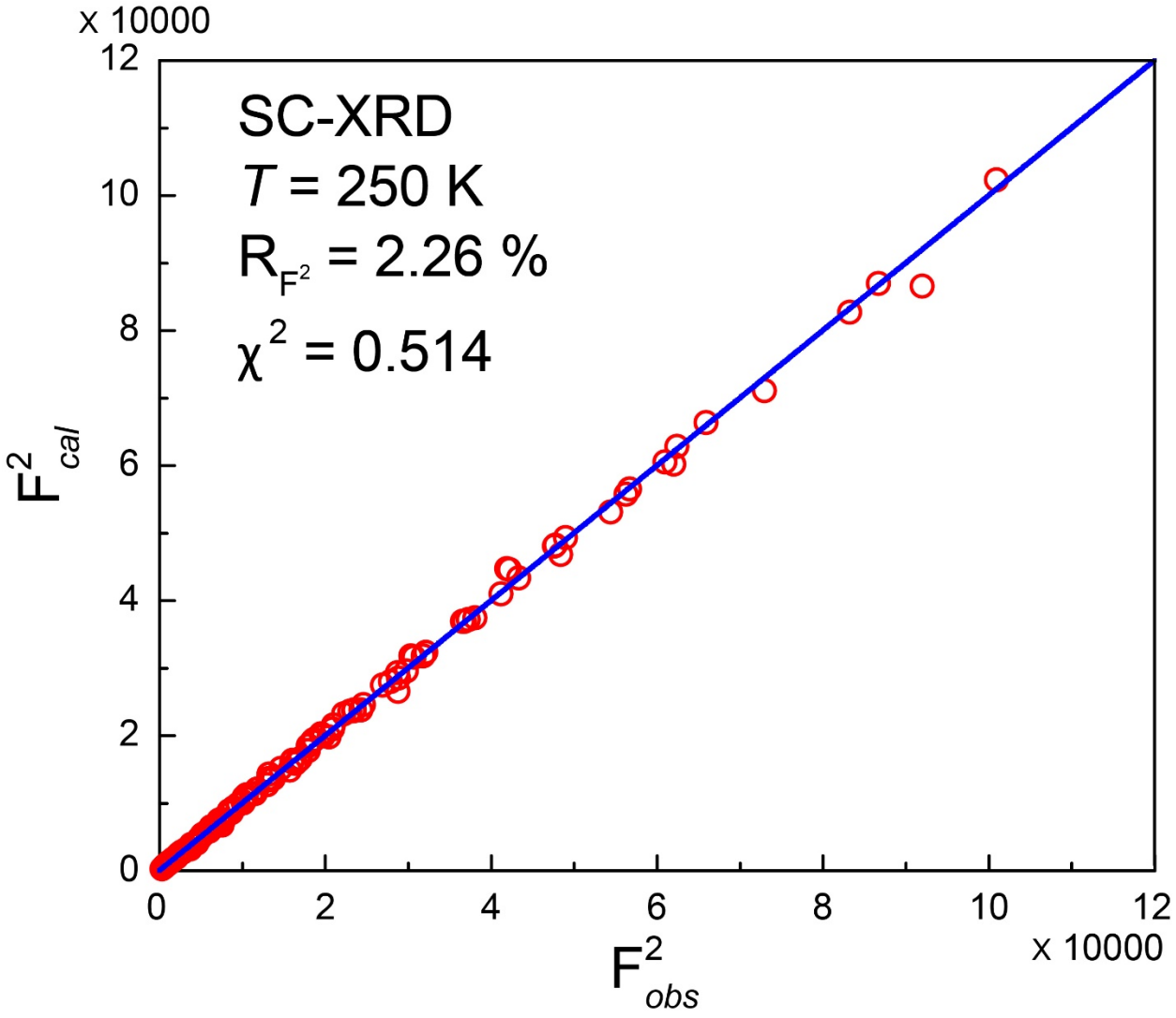

Figure S4. Observed and calculated refinement results using single crystal Rietveld analysis for crystal #1. Similar results are obtained for crystal #2.

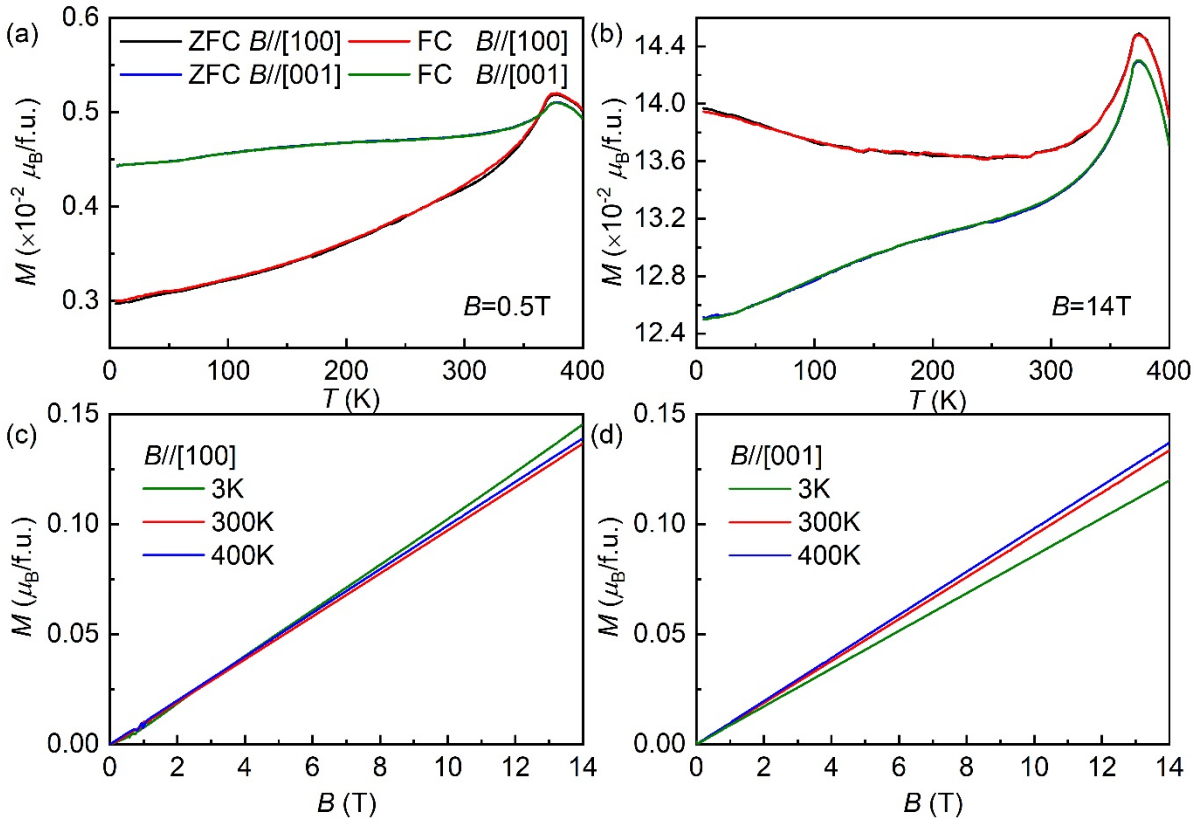

Figure S5. Temperature dependence of magnetization $M(T)$ at (a) 0.5 T and (b) 14 T for H//[100] and H//[001] with zero-field cooling and field-cooling modes. Field dependence of magnetization $M(B)$ at T = 3 K, 300 K and 400 K for (c) H//[100] and (d) H//[001]. It shows an antiferromagnetic transition at about T_N ~ 377 K under a magnetic field of B = 0.5 T.

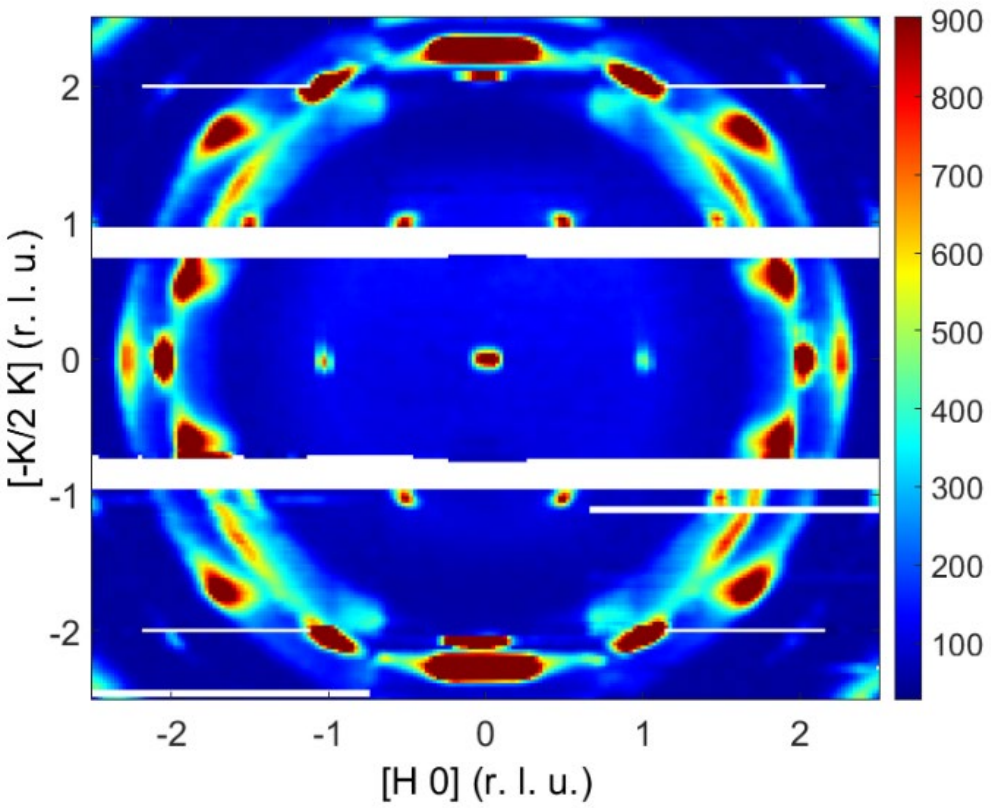

Figure S6. Mosaic of FeSn single crystal assembly. Elastic peak patterns in the [*H*, *K*] plane with *L* integrated between [-1, 1], where one can see Bragg peaks at the right positions with in-plane mosaic full width at half maximum FWHM = 6.1°.

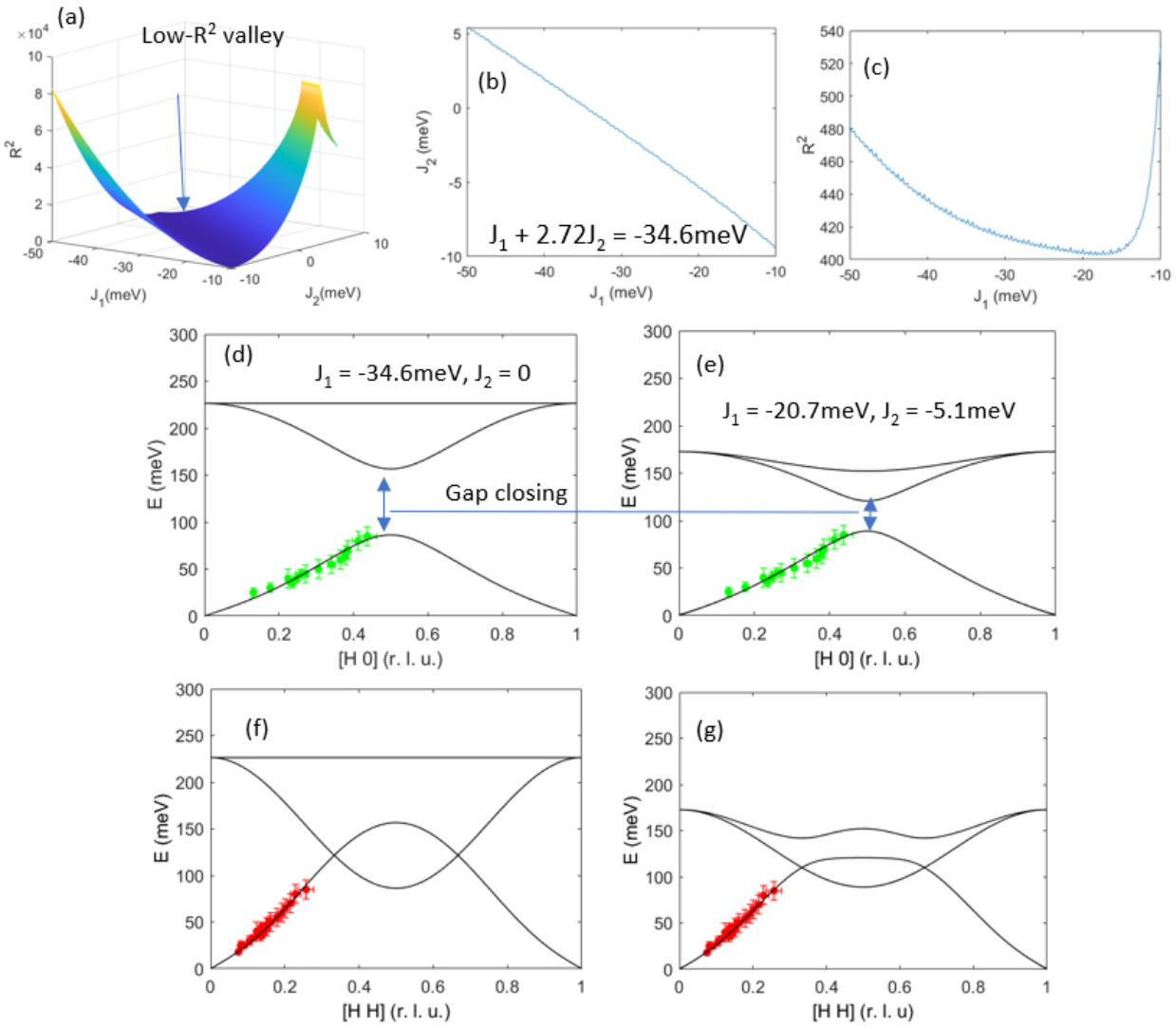

Figure S7. Least-square error fit of the spin wave spectrum. (a) Relationship between each [J_1, J_2] pair and corresponding square error R^2, showing a valley with low R^2 values; (b) The projection of the valley on [J_1, J_2] plane, showing a linear relation between these two J's; (c) The projection of the valley on [J_1, R^2] plane. Note that the R^2 value is kept low; (d-g) Fitted spectrum along [H,0] (d, e) and [H,H] (f, g) direction with J_1-only model (d, f) and the J_1-J_2 model discussed in the main text (e, g). Note that the spin gap size between acoustic and optic mode at M point (0.5,0) changes with J_2, thus giving us an opportunity to determine the correct [J_1, J_2] pair more accurately.

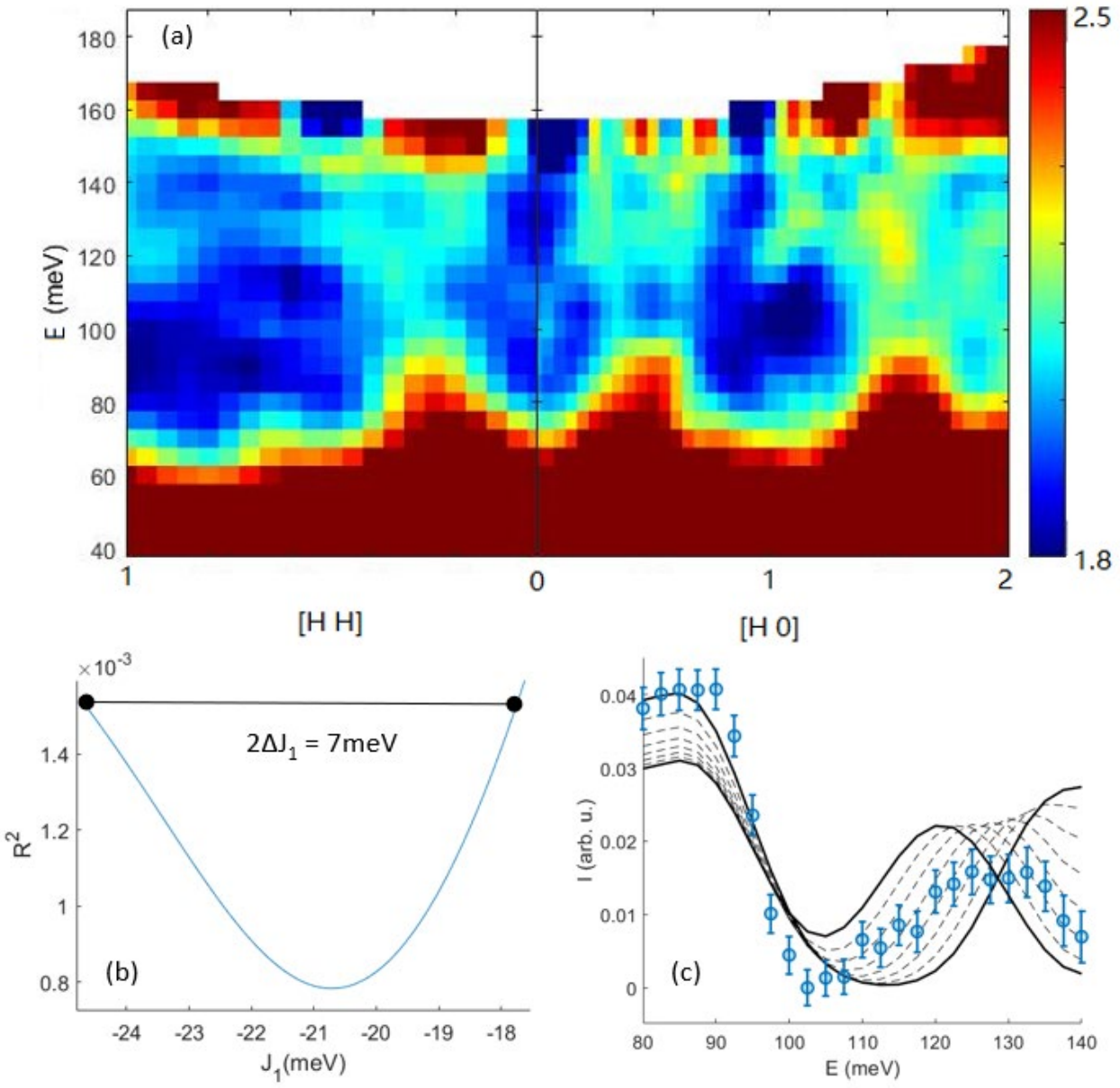

Figure S8. Least-square error fit of the spin wave spectrum at the *M* point. (a) Spin wave spectrum along the [*H*,*H*] and [*H*,0] directions. The acoustic and optical modes cross at *K* point (1/3,1/3) without a gap, while a ~10 meV gap occurs at the *M* point (1/2,0). (b) Relationship between squared error and J_1, here J_2 is calculated by $J_1+2.72J_2$ = -34.6meV. The error of J_1 is determined by the range of J_1 where the squared error is below twice of the minimum squared error. (c) The fitting spectrum. Data (blue circles) is the same as in the Fig. 2(b) of the main text. Areas filled by black dashed lines is the coverage of the spectrum generated by range [$J_{1opt} - \Delta J_1$, $J_{1opt} + \Delta J_1$], where J_{1opt} is the fitted optimum J_1 value. The black solid line shows the fit generated by $J_{1opt} - \Delta J_1$ and $J_{1opt} + \Delta J_1$.

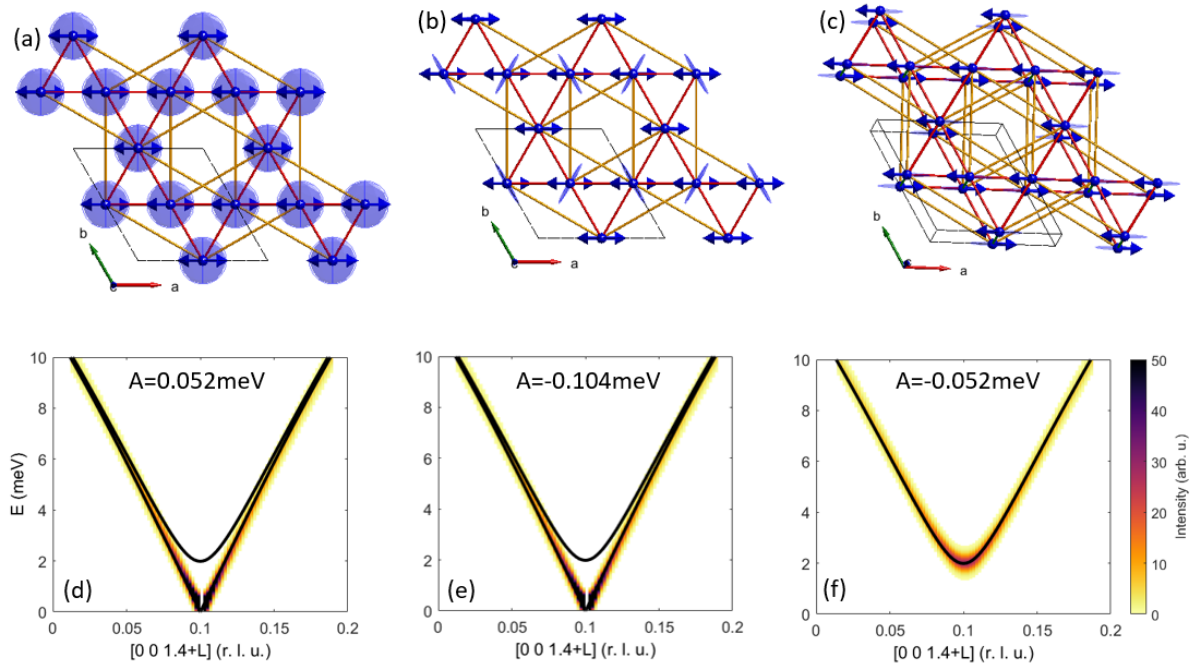

Figure S9. Magnetic anisotropy and its relationship with the spin gap at Γ point. Here we assume spin direction along **a** which is parallel to *x*. Red and yellow lines represent J_1 and J_2, respectively. (a) XY-type anisotropy. $H = A(S_z)^2$ with A>0. (b) Single-ion anisotropy respecting lattice symmetry. $H = A(S_{\hat{e}(\mathbf{r})})^2$ with A<0. The easy axis $\hat{e}(\mathbf{r})$ is dependent on atomic position **r** as shown in the anisotropy ellipsoid (blue). (c) Dipole-like anisotropy breaking lattice symmetry. $H = A(S_x)^2$ with A<0. (d-f) Spin excitation spectrum at around AF **Q**-vector (0,0,1.5) generated by anisotropies in (a-c), respectively. The solid black lines show the dispersion relation, and the color bar shows the calculated neutron structure factor. While all models have a band located at E = 1.99 meV at (0,0,1.5), only the band in (f) shows non-zero structure factor that can be observed by INS.

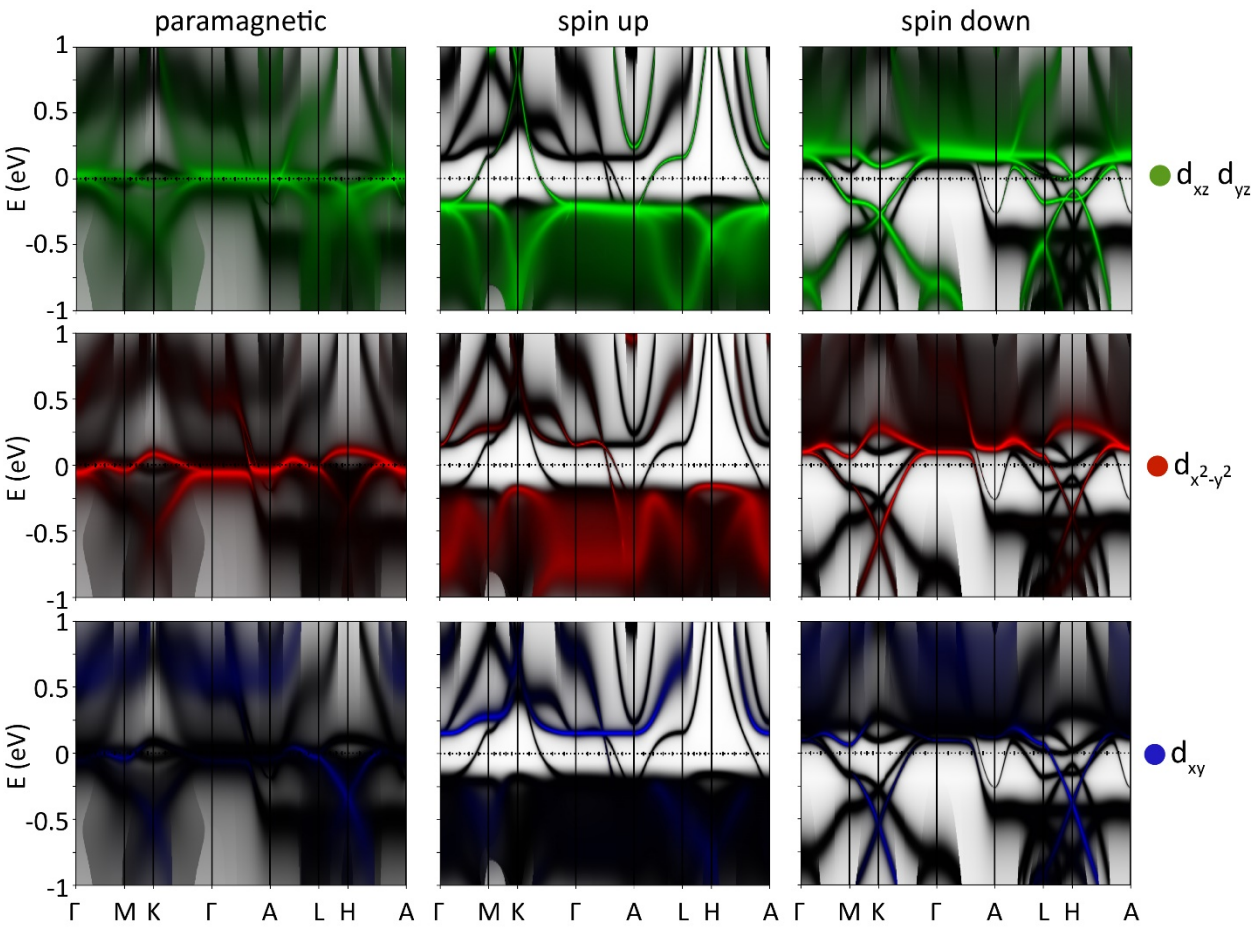

Figure S10. DFT+DMFT calculated orbital-resolved band structures of FeSn in the paramagnetic, spin up, and spin down magnetically ordered state, respectively. Green color is the contribution from the d_{xz} and d_{yz} orbitals. Red, blue, and black colors represent $d_{x^2-y^2}$, d_{xy}, and d_{z^2} orbitals, respectively.

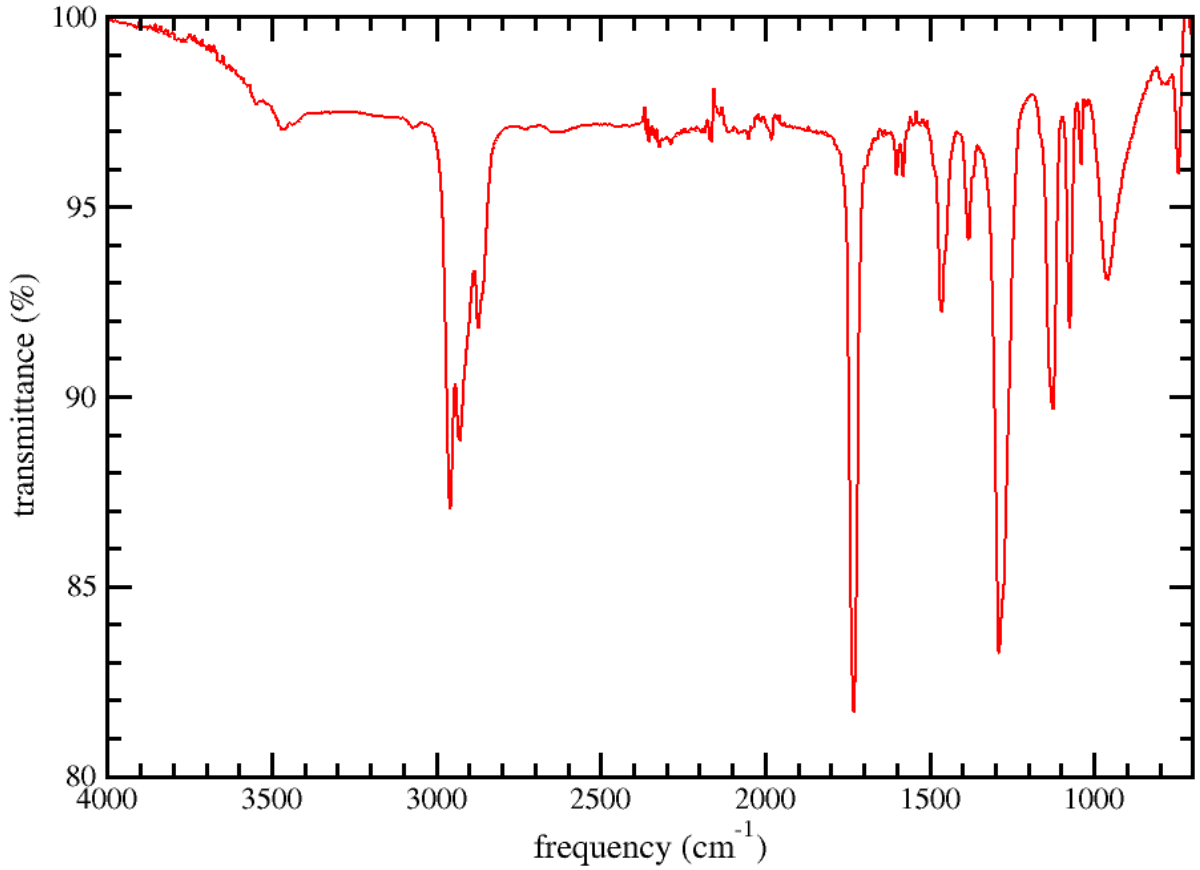

Figure S11. The infrared absorption spectrum in the figure above was collected on a Jasco FT/IR 6600 Fourier Transform Infrared (FTIR) spectrometer equipped with an ATR (Attenuated Total Reflectance) attachment with a diamond anvil. The dynamic range used was 4000-700 cm^{-1} with a resolution of 4 cm^{-1}. To reduce noise, 64 scans were averaged to produce the absorption spectrum. No corrections were applied other than the sloping baseline due to strong light reflection on the aluminum support. The 0.5×0.5 cm^2 sample was cut out of the aluminum foil and the side exposed to the contaminant was placed directly on the ATR attachment and pressed on the diamond window. The data were collected at room temperature and the instrument was not flushed with an inert gas. A sample of the same aluminum foil not exposed to the contaminant was measured and produced no signal other than a continuous sloping background due to light reflection on the metallic foil.